A two-dimensional dislocation model for interseismic deformation of the Taiwan mountain belt

Ya-Ju Hsu [a,b,c,*], Mark Simons [c], Shui-Beih Yu [a], Long-Chen Kuo [a], Horng-Yue Chen [a]

[a] *Institute of Earth Sciences, Academia Sinica, P.O. Box 1-55, Nankang, Taipei, Taiwan*
[b] *Institute of Geophysics, National Central University, Chungli, Taiwan*
[c] *Seismological Laboratory, Division of Geological and Planetary Sciences, California Institute of Technology, Pasadena, CA 91125, USA*

Abstract

We use a Global Positioning System (GPS)-derived surface velocity field of Taiwan for the time period between 1993 and 1999 to infer interseismic slip rates on subsurface faults. We adopt a composite elastic half-space dislocation model constrained by the observed horizontal velocities projected into the direction of plate motion (306°). The GPS data are divided into northern and southern regions and the velocities in each region are projected into single profiles. The model fault geometry includes a shallowly dipping décollement, based on the balanced geological cross-sections in the Coastal Plain and Western Foothills, and a two-segment fault representing the Longitudinal Valley Fault (LVF) in eastern Taiwan. The décollement is composed of two fault segments, one extending west under the Central Range (CR) and one extending east of the LVF, with estimated slip rates of about 35 and 80 mm/yr, respectively. The optimal geometry of décollement is subhorizontal (2°∼11°) at a depth of 8∼9 km. The inferred surface location of the western end point of dislocation in the northern profile is located 15 km east of the Chelungpu Fault, while in the southern section, it is located beneath the Chukou Fault. The elastic dislocation model successfully matches the horizontal velocity data, and predicts elastic strain accumulation in the Western Foothills that will presumably be released in future earthquakes. However, considered over multiple earthquake cycles, our model cannot explain the topography of the CR and thus fails to predict the active mountain building process in Taiwan. This failure indicates that both horizontal and vertical velocity fields require a more complex rheological model that incorporates inelastic behavior.
© 2003 Elsevier Science B.V. All rights reserved.

Keywords: Taiwan; global positioning system; strain; Chi-Chi; crustal deformation; Central Range

1. Introduction

Taiwan is located on the Eurasian continental margin bounded by two subduction zones. In the north, the Philippine Sea Plate (PSP) subducts beneath the Ryukyu Arc, while to the south, the

---

* Corresponding author. Tel.: +886-2-27839910 ext. 415; Fax: +886-2-27839871.
 E-mail address: yaru@earth.sinica.edu.tw (Y.-J. Hsu).
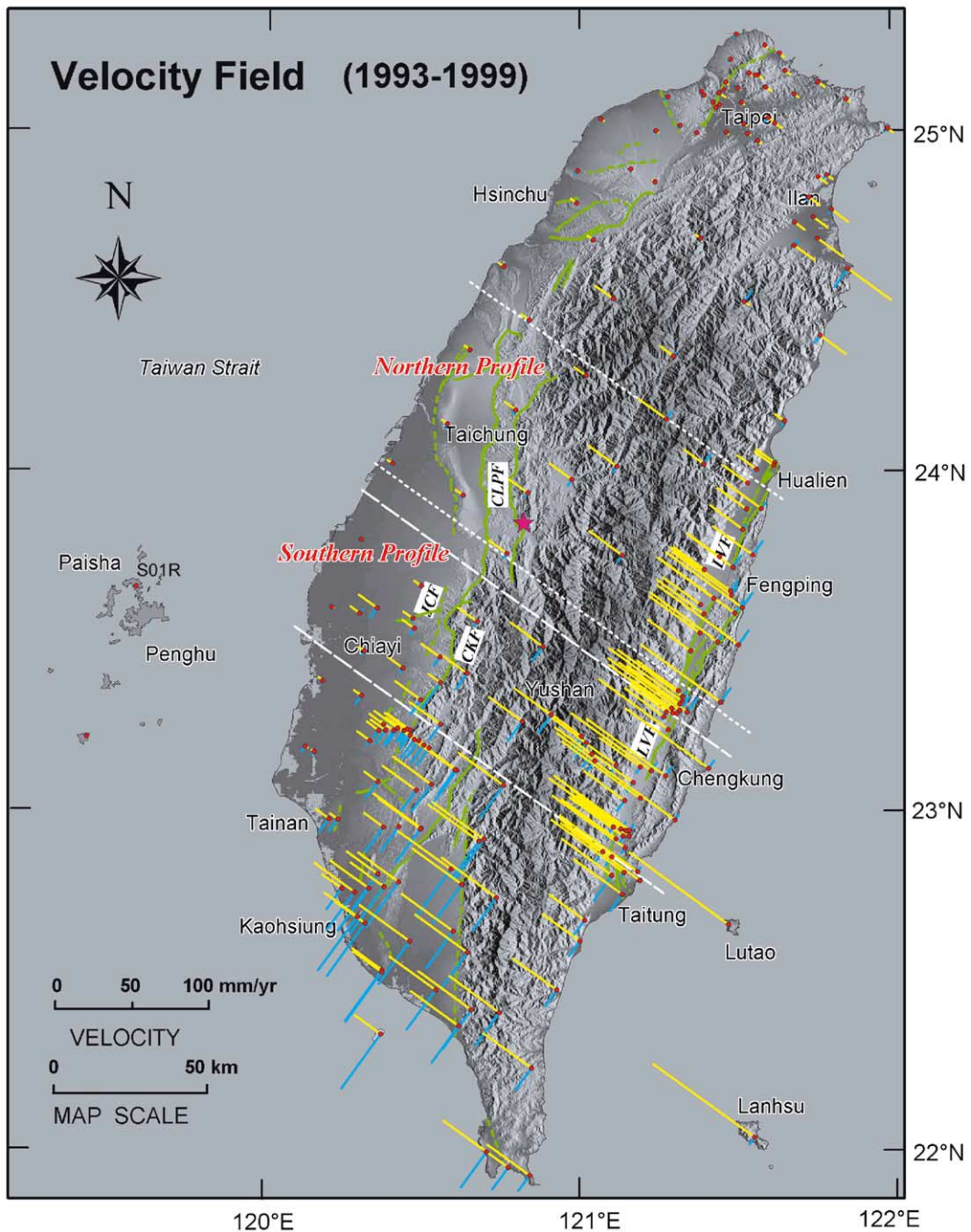
Fig. 1. Shaded relief topographic map of Taiwan. Major faults are indicated as green lines. Red dots correspond to GPS stations, with yellow and blue lines indicating GPS velocities projected parallel and normal to the direction of plate motion. The short-dash and long-dash lines denote the northern and southern sections, respectively. The pink star indicates the epicenter of the Chi-Chi earthquake.

Eurasian Plate (EP) subducts beneath the PSP. Convergence between the PSP and the EP drives collision of the Luzon Arc with the Chinese continental margin. The arc–continent collision in northern Taiwan has ceased and the major zone of collision is gradually moving southward. The total convergence rate across the collision zone is about 80 mm/yr in a 306° direction [1,2]. The bulk of the implied strain occurs in Taiwan and produces the Coastal Range, the Central Range (CR), with elevations close to 4000 m, and the fold-and-thrust belt in western Taiwan.

Using data from the Taiwan Global Positioning System (GPS) network, observed periodically since 1990, we have an opportunity to delineate the overall deformation pattern. Analyzing data collected between 1993 and 1999 (Fig. 1), convergent strain accumulation appears to be partitioned into two major zones, the fold-and-thrust belt in the Western Foothills and the Longitudinal Valley Fault (LVF) in eastern Taiwan. The east–west shortening rate of between 30 and 40 mm/yr in SW Taiwan occurs in one of the most seismically active regions, where over 18 major earthquakes with magnitudes greater than 6 have occurred since 1900. On the eastern side of the CR, the NNE-striking LVF is a high angle thrust and is considered to be the active plate boundary between the EP and the PSP. The velocity discontinuity across the LVF is about 30 mm/yr; a large part of which is attributed to shallow aseismic slip on the fault [1,3].

Ding et al. [4] used an elasto-plastic finite element model framed in the context of a thin-skinned model for the Taiwan orogeny. Their model agrees with the major features of GPS horizontal data, however they predict NW–SE extension in the CR, different from NE–SW extension inferred from GPS data [1] and earthquake focal mechanisms [5]. Furthermore, the absolute magnitudes of the vertical displacements in their model do not agree with inferences based on present-day topography. While finite element models permit exploitation of realistic rheologies, the associated computational burden currently makes their use in optimization problems prohibitive. Loevenbruck et al. [6] and Dominguez et al. [7] used buried elastic dislocation models to interpret interseismic deformation in central Taiwan. Their models successfully fit the first-order features of the velocity field. But neither study attempted to use GPS data to invert for fault geometry, as we do, based on geologic constraints. In this study, we use an updated GPS velocity field with about twice the number of GPS stations used in previous studies [8]. Our model is similar to the previously derived elastic dislocation models, and assumes a nearly horizontal dislocation (décollement) as a proxy for a deep creeping zone. This approach has also been applied to other collision zones (e.g. [9,10]). We conclude with an assessment of both the successes and the failures of such a décollement model in explaining the primary observations of crustal deformation in Taiwan.

2. Data collection and analysis

We use velocity data from a dense GPS network collected between 1993 and 1999, before the 1999 Chi-Chi earthquake (M_w 7.6) [8]. This data set consists of 190 annually surveyed and 25 continuously recording stations (Fig. 1). Most campaign-surveyed stations are observed at least once per year. We decompose the horizontal GPS station velocity vectors into components parallel (V_{par}) and normal (V_{norm}) to the plate motion. Several first-order features are immediately evident in the projected velocities (Fig. 1). V_{par} is discontinuous across the LVF, and then maintains nearly the same magnitude across the CR until reaching the Western Foothills. Velocities gradually decrease in the western Coastal Plain and reach a more or less constant value at Penghu Island. The east–west shortening rate in the Western Foothills changes significantly from about 20 mm/yr in central Taiwan, where the Chi-Chi earthquake occurred, to about 40 mm/yr in southwestern Taiwan. In general, V_{norm} increases southward suggesting lateral extrusion of southern Taiwan. Finally, we see southeastward movement in northeastern Taiwan, inferred to be the result of extensional deformation due to the opening of Okinawa Trough [11].

We use projected horizontal GPS velocities to

constrain simplified two-dimensional models (Fig. 3c,d). The surface traces of major faults in our two sections are roughly perpendicular to the direction of plate motion (Fig. 1), justifying the initial use of two-dimensional models. The GPS data between 23°N and 24.5°N are divided into two sections according to geological setting. The locations of both sections are shown in Fig. 1. The northern section contains 31 campaign-surveyed and two permanent stations, while the southern section contains 32 campaign-surveyed and five permanent stations. They include the regions traversed by the Chelungpu Fault (CLPF), the Chukou Fault (CKF) and Jiuchiungken Fault (JCF). The widths of the northern and southern sections are 70 and 40 km, respectively. A velocity discontinuity of about 25 mm/yr is clearly evident in Fig. 3c,d, which we associate with the LVF. We also observe a change of about 25 mm/yr across the Western Foothills and Coastal Plain (a 60-km-wide belt).

3. Two-dimensional buried dislocation model

The observed strain may be due to both elastic and inelastic processes. Here, we address the viability of a purely elastic model with slip on buried dislocations. Our adopted fault geometries are determined by geological constraints. Based on deep drilling, seismic reflection profiles, surface mapping and balanced cross-sections, the fold-and-thrust belt in western Taiwan has been previously modeled using a critical taper wedge model [12]. The model adopts a dip for the basal décollement of about 6° to the east. Mouthereau et al. [13]

inferred a mixed thin- and thick-skinned model, based on tectono-sedimentary analyses and balanced cross-sections in SW Taiwan. A shallow aseismic décollement is estimated to exist at a depth of 6–8 km, attributed to a thick Late Miocene shale unit that is expected to deform inelastically. A deeper décollement is also inferred to exist, at depths of 12–15 km, based on seismicity and focal mechanisms [14,15]. Carena et al. [16] used over 10^5 small earthquakes to identify a detachment at about 10 km depth, with the shape of the detachment controlling first-order features in the topography. Studies of aftershocks from the Chi-Chi earthquake also find a nearly horizontal plane at depths between 8 and 12 km [17,18], which may correspond to a décollement. Hsu et al. [19] inverted for the fault geometry and afterslip of the Chi-Chi earthquake based on the postseismic GPS displacements, and concluded that significant slip occurred on the nearly horizontal décollement at a depth of about 8–12 km. Based on this ensemble of observations, we assume a fault geometry (Fig. 2) that includes a shallowly dipping décollement (S_3) at depths between 6 and 15 km to account for aseismic slip in the interseismic period. We also use an infinite horizontal dislocation (S_4) to represent the northwestward movement of the PSP. The slip rate on S_4 is constrained a priori to be about 80 mm/yr. Deformation in the partly locked LVF is represented by two patches (S_1 and S_2), with the upper patch extending to the surface. In the LVF, the width of the creeping zone is narrow (less than 2 km) with approximately equal vertical and horizontal creeping rates of about 24 mm/yr [20]. Projections of small earthquake hypocenters across the LVF
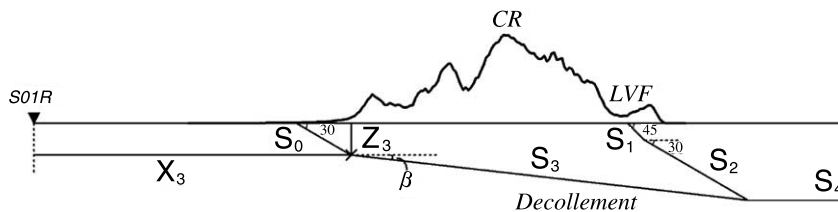
Fig. 2. A schematic of the assumed fault geometry of our two-dimensional interseismic dislocation model. Topography is shown with 6× vertical exaggeration. S_0 denotes the suggested fault for a future rupture. S_1 and S_2 correspond to two segments of the LVF, while S_3 and S_4 correspond to two segments of the buried dislocations in the west and east of the LVF, respectively. β is the dip of S_3. (X_3, Z_3) denote the end point of the buried dislocation. CR indicates the Central Range.
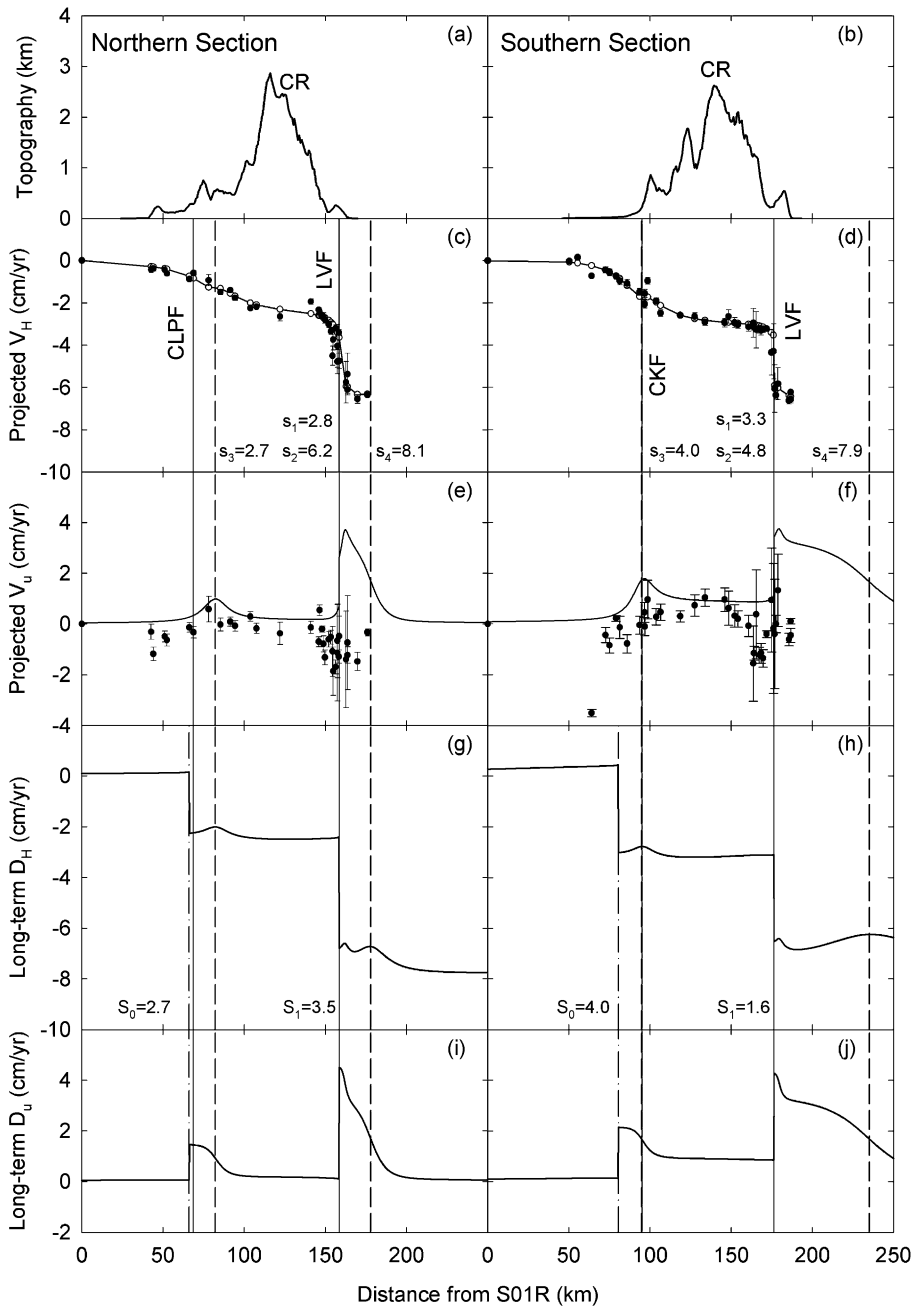
Fig. 3. Comparison of observations and predictions from the best-fit composite dislocation model. The left and right columns correspond to the northern and southern profiles, respectively. (a,b) Topography. (c,d) Horizontal velocities. (e,f) Vertical velocities. Solid circles with error bars are the observed velocities, while the curves with open circles represent the optimal model. S_1, S_2, S_3 and S_4 represent slip rates (cm/yr) on each fault patch. CLPF, CKF, and LVF (solid lines) denote the Chelungpu Fault, Chukou Fault and Longitudinal Valley Fault, respectively. Dashed lines represent the location of two patches of buried dislocations. (g,h) Predicted long-term horizontal and (i,j) vertical displacement rates. Dash–dot lines indicate the suggested location (S_0) for a future rupture.

suggest a listric east-dipping fault (Rau, personal communication), therefore we assume dip angles of 45° and 30° for the upper and lower segments, respectively.

Due to present limitations of our knowledge of fault geometries, we invert for both fault slip rates and perturbations from our initial geometry, using a grid search approach, to obtain an optimal set of fault parameters. This method does not directly provide correlation coefficients between all of the parameters. To make first-order estimates of the correlation coefficients, we use a non-linear search approach. The starting fault parameters for the non-linear search are obtained from the estimate of the prior grid search. We estimate optimal fault parameters and their 95% confidence intervals using a bootstrap method. We resample the actual data set **d**, with its *N* stations, to generate 1000 synthetic data sets **d₁**, **d₂**, **d₃** … **d₁₀₀₀**, also with *N* stations. Some stations may be chosen multiple times, others not at all. We subject these sampled data sets to the same estimation procedure as is performed on the actual data. Finally, we generate the distribution of fault parameters. The global optimal solution and 95% confidence intervals are given in Table 1. The observed GPS velocity values, and model values predicted from the optimal solutions, are shown in Fig. 3.

4. Results and discussion

Despite the simple fault geometry assumed, our model fits the projected horizontal GPS velocities (Fig. 3c,d). The two sections show similar values of the inferred dipping angle (2–11°) and depth (8–9 km) of the décollement. In the northern sec-

tion, if a 30° east-dipping fault connects to the end point of dislocation to the surface (S_0 in Fig. 2), the implied fault trace is approximately on the CLPF, where the 1999 M_w 7.6 Chi-Chi earthquake occurred. In the southern section, the end point of dislocation is located beneath the CKF, implying that future rupture in the southern section should be to the west of the CKF. The interseismic slip rates (Fig. 3c,d) on the décollement are 27 and 40 mm/yr in the northern and southern sections, respectively. More strain is accumulating in southern Taiwan, in agreement with historical earthquake records [21]. However, the inferred interseismic slip rate may not necessarily represent long-term rates [13].

We use our inferred model derived from horizontal GPS data to predict vertical velocities (Fig. 3e,f). The observed vertical component of the GPS data is considerably more scattered than the horizontal component. However, in both profiles, the observed data indicate finite uplift of the CR relative to the coasts, over a spatial extent of approximately 70 km. In the southern section, bracketed by the CKF and the LVF, relative uplift rates reach a maximum near the highest part of the CR, with a peak rate of approximately 15 mm/yr. Uplift in the northern section is more subdued. Our model predictions, either considered in terms of the interseismic phase (Fig. 3e,f) or integrated over many earthquake cycles (Fig. 3i,j), are not consistent with the vertical GPS data except for the predicted uplift trends in western Taiwan at distances between 50 and 100 km (Fig. 3e,f), which generally fit the GPS data. We construct our predicted long-term horizontal and vertical geological rates by assuming all the inferred buried slip reaches the surface. Besides problems with fitting the vertical GPS data, our models

Table 1
Optimal fault parameters and 95% confidence intervals for both northern and southern sections

	Fixed parameters				Optimal parameters		
	Z_1 (km)	β_1 (deg)	Z_2 (deg)	β_2 (deg)	X_3 (km)	Z_3 (km)	β_3 (deg)
North	0	45	3	30	82.0 ± 7.2	9.2 ± 3.2	2.0 ± 2.6
South	0	45	3	30	94.9 ± 3.1	8.3 ± 2.9	10.9 ± 9.7

Z_1, Z_2 and Z_3 represent the depths of upper edges for fault segment 1, 2, 3, respectively. β_1 and β_2 are the dip angles. (X_3, Z_3) is the location of the end point of dislocation. β_3 is the dip angle of S_3. See Fig. 2 for the location of each fault.

predict the surface vertical deformation is about 4 cm/yr in the LVF while the leveling data across the LVF show a vertical creeping rate of about 2.4 cm/yr [20]. This misfit may be due to uncertainties in the fault geometries used.

Loevenbruck et al. [6] used elastic dislocations to simulate aseismic slip on a 10-km-deep décollement. They assumed a creeping LVF and a flat décollement with slip rates of 35 and 45 mm/yr, respectively. Their model underestimates the projected velocities in Western Foothills and overestimates them in the LVF. Part of this misfit is due to the values assumed for the dip angles of the fault segments. Their assumed geometry results in large variations of the projected GPS horizontal velocities in the CR, a feature that is not seen in the GPS observations. Using the thermal model from Lin [22], Dominguez et al. [7] assumed a horizontal shear zone at about 12 km depth. They used GPS data to estimate an interseismic slip rate of about 40 mm/yr. Based on the distribution of seismicity before the Chi-Chi earthquake, they concluded that the western edge of the creeping zones lies at least 40 km east of the CLPF, near the eastern edge of the Sun Moon Lake seismic gap, an area that is seismically quiescent. Our inversion for the optimal fault geometry suggests that the location is about 15 km east of CLPF. Dominguez et al. [7] suggest that the Chi-Chi earthquake did not rupture the entire locked fault. In contrast, if we assume a 30° east-dipping fault extending from the end of dislocation to the surface, the fault projects right to the CLPF, suggesting that the Chi-Chi earthquake may have released the greater part of stored elastic strain in this region. We estimate a correlation coefficient between X_3 and Z_3 close to 1. Such a strong trade-off between the horizontal position (X_3) and the depth (Z_3) of the end of dislocation can explain the discrepancy between the Dominguez et al. results and our results.

Our simple model combines a priori information from geology and seismology and searches for optimal parameters using a bootstrap method. We estimate localized slip along a thrust and the décollement along with an optimal geometry. This model is only a proxy for any ductile shear on the décollement under the CR. Vergne et al. [23] compared many previous studies of interseismic deformation with a more realistic two-dimensional finite element model in the Himalayas. They concluded the meaningful parameters in the buried dislocation model are the position of the end of dislocation and the dip angle of the lower décollement. Their results may highlight the limitations of our model.

5. Conclusion

We use two-dimensional elastic dislocation models to interpret the GPS velocity field between 1993 and 1999. Our model fits the horizontal GPS velocities very well with the optimal fault geometry including a subhorizontal décollement ($2° \sim 11°$) at a depth of $8 \sim 9$ km and two fault segments in the LVF. We estimate the western edge of décollement and predict that the location of possible future rupture in the southern section will be located west of the CKF. In the northern section, the surface rupture is expected to be on the CLPF that ruptured during the 1999 Chi-Chi earthquake. However, our model does not fit the vertical GPS velocities very well. Over multiple earthquake cycles, our model predicts no localized strain or uplift under the CR. The lack of predicted uplift in the CR is characteristic of any model in which most of the convergence is transferred across Taiwan to the Western Foothills. This inconsistency with observed long-term geology highlights the inherent non-uniqueness of models fitting only horizontal data and suggests the need for a more complex model that incorporates inelastic behavior.

References

[1] S.B. Yu, H.Y. Chen, L.C. Kuo, Velocity field of GPS stations in the Taiwan Area, Tectonophysics 274 (1997) 41–59.

[2] S.B. Yu, L.C. Kuo, R.S. Punongbayan, E.G. Ramos, GPS observation of crustal motion in the Taiwan-Luzon region, Geophys. Res. Lett. 26 (1999) 923–926.

[3] S.B. Yu, D.D. Jackson, G.K. Yu, C.C. Liu, Dislocation model for crustal deformation in the Longitudinal Valley area, eastern Taiwan, Tectonophysics 183 (1990) 97–109.

[4] Z.Y. Ding, Y.Q. Yang, Z.X. Yao, G.H. Zhang, A thin-skinned collisional model for the Taiwan orogeny, Tectonophysics 332 (2001) 321–331.

[5] H. Kao, P.R. Jian, Seismogenic patterns in the Taiwan region insights from source parameter inversion of BATS data, Tectonophysics 333 (2001) 179–198.

[6] A. Loevenbruck, R. Cattin, X. LePichon, M.L. Courty, S.B. Yu, Seismic cycle in Taiwan derived from GPS measurements, C.R. Acad. Sci. II 333 (2001) 57–64.

[7] S. Dominguez, J.P. Avouac, R. Michel, Horizontal coseismic deformation of the 1999 Chi-Chi earthquake measured from SPOT satellite images: implications for the seismic cycle along the western foothills of Central Taiwan, J. Geophys. Res. (2003) in press.

[8] S.B. Yu, L.C. Kuo, Y.J. Hsu, H.Y. Chen, Interseismic crustal deformation in the Taiwan plate boundary zone (1993–1999), in preparation.

[9] M. Jackson, R. Bilham, Constraints on Himalaya deformation inferred from vertical velocity fields in Nepal and Tibet, J. Geophys. Res. 99 (1994) 13897–13912.

[10] K. Larson, R. Burgmann, R. Bilham, J.T. Freymuller, Kinematics of the India-Eurasia collision zone from GPS measurements, J. Geophys. Res. 104 (1999) 1077–1093.

[11] C.C. Liu, The Ilan Plain and the southwestward extending Okinawa Trough, J. Geol. Soc. China 3 (1995) 183–193.

[12] J. Suppe, Imbricated structure of western foothills belt, southcentral Taiwan, Petrol. Geol. Taiwan 17 (1980) 1–16.

[13] F. Mouthereau, O. Lacombe, B. Deffontaines, J. Angelier, S. Brusset, Deformation history of the southwestern Taiwan foreland thrust belt insights from tectono-sedimentary analyses and balanced cross-sections, Tectonophysics 333 (2001) 293–322.

[14] R.J. Rau, F.T. Wu, Active tectonics of Taiwan orogeny from focal mechanisms of small-to-moderate sized earthquakes, TAO 9 (1998) 755–778.

[15] A. Lacombe, F. Mouthereau, J. Angelier, B. Deffontaines, Structural, geodetic and seismological evidence for tectonic escape in SW Taiwan, Tectonophysics 333 (2001) 323–345.

[16] S. Carena, J. Suppe, H. Kao, Active detachment of Taiwan illuminated by small earthquakes and its control of first-order topography, Geology 30 (2002) 935–938.

[17] N. Hirata, S. Sakai, Z.S. Liaw, Y.B. Tsai, S.B. Yu, Aftershock observations of the 1999 Chi-Chi, Taiwan earthquake, Bull. Earthq. Res. Inst. Tokyo Univ. 75 (2000) 33–46.

[18] K.C. Chen, B.S. Huang, J.H. Wang, H.Y. Yen, Conjugate thrust faulting associated with the 1999 Chi-Chi Taiwan, earthquake sequence, Geophys. Res. Lett. 29 (2002) 10.1029/2001GL014250.

[19] Y.J. Hsu, N. Bechor, P. Segall, S.B. Yu, L.C. Kao, K.F. Ma, Rapid afterslip following the 1999 Chi-Chi Taiwan earthquake, Geophys, Res. Lett. 29 (2002) 10.1029/2002GL014967.

[20] S.B. Yu, L.C. Kuo, Present-day crustal motion along the Longitudinal Valley Fault, eastern Taiwan, Tectonophysics 333 (2001) 199–217.

[21] S.N. Cheng, Y.T. Yeh, M.T. Hsu, T.C. Shin, Photo album of ten disastrous earthquakes in Taiwan, CWB-9-1999-002-9, 1999, 290 pp. (in Chinese).

[22] C.H. Lin, Thermal modeling of continental subduction and exhumation constrained by heat flow and seismicity in Taiwan, Tectonophysics 324 (2000) 189–201.

[23] J. Vergne, R. Cattin, J.P. Avouac, On the use of dislocations to model interseismic strain and stress build-up at intracontinental thrust faults, Geophys. J. Int. 147 (2001) 155–162.